THE JOURNAL OF PHYSICAL CHEMISTRY C

Article

pubs.acs.org/JPCC

Piezoelectrochemical Effect: A New Mechanism for Azo Dye Decolorization in Aqueous Solution through Vibrating Piezoelectric Microfibers

Kuang-Sheng Hong,[†] Huifang Xu,*[,†] Hiromi Konishi,[†] and Xiaochun Li[‡]

[†]Department of Geoscience and [‡]Department of Mechanical Engineering, Materials Science Program, University of Wisconsin—Madison, 1215 West Dayton Street, Madison, Wisconsin 53706, United States

ABSTRACT: A newly discovered piezoelectrochemical (PZEC) effect for the direct conversion of mechanical energy to chemical energy is applied for the mechanically induced degradation of a dye of C.I. Acid Orange (AO7) from aqueous solution in the presence of $BaTiO_3$ microdendrites. The mechanism of the PZEC degradation of the dye depends on the ultrasonic vibration used, in which the formation of the strain-induced electric charges on the dendrite surface is due to the deformation and local charge accumulation on the $BaTiO_3$. With sufficient applied electric potential, strained piezoelectric dendrites in AO7 aqueous solution triggered the decomposition reaction. The process is monitored by following the decolorization rate of AO7. The effects of pH, catalyst loading, and initial dye concentration on dye degradation were also studied. Kinetic analyses reveal that the PZEC degradation rates of AO7 can be approximated in terms of the Langmuir−Hinshelwood model. The value of the adsorption equilibrium constant, K_{AO7}, was 0.149 $(mgl^{-1})^{-1}$, and the value of the kinetic rate constant of the surface reaction, k_c, was 0.50 mgl^{-1} min^{-1}. These new strain-induced chemical reactions can provide a simple and cost-effective technology for decomposing organic pollutants in aqueous solution by scavenging waste energy such as noise or stray environmental vibrations.

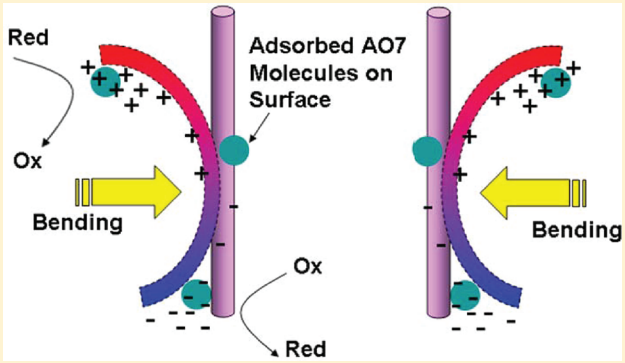

INTRODUCTION

Decolorization of dye has received significant attention due to the increasing environmental protection demands on the removal of pollution and eutrophication sources in waste waters. These pollutants may generate dangerous byproducts through chemical reactions in the wastewater phase.[1−5] Traditionally, physical techniques, including adsorption on activated carbon, ultrafiltration, reverse osmosis, and ion exchange on synthetic adsorbent resins among others, are utilized to remove the pollutants. However, these non-destructive physical techniques usually result in the transfer of the pollutants from water to another phase, which could easily cause secondary pollution.[6−8] Biological treatment methods have been reported and found to be ineffective for decolorization and degradation due to the large degree of aromatics present in dye molecules and the stabilities of modern dyes.[9−11] Ozonation and chlorination have also been used but often have high operating costs and slower reaction rates.[8,12,13] Advanced oxidation processes (AOPs) are alternative technologies for dye destruction.[14−17] In recent years, AOPs, TiO_2, and ZnO have been used as effective, nontoxic, and inexpensive semiconductor photocatalysts for the degradation of organic chemicals and dyes.[18−25] Nevertheless, semiconductor based materials have limitations in conditional usage and solar efficiency. Additionally, corrosion may occur for these photocatalysts under low pH conditions,[26] which could lower the degradation efficiency of the dyes for these applications.

In this study, we report the discovery of a phenomenon—the direct conversion of mechanical energy to chemical energy, termed the piezoelectrochemical (PZEC) effect, for a mechanism of dye decomposition relying upon the piezoelectric properties of the catalysts.[27] Accordingly, we report the findings of our research on tetragonal barium titanate ($BaTiO_3$, *P4mm*) along with the external mechanical force, to drive the decomposition of methyl orange dye in aqueous solution. From the study, we would like to demonstrate the potential capabilities of this material for scavenging waste energy from the environment, such as noise and vibration, to initiate oxidation−reduction reactions of the absorbents, and further to be applied for environmental cleaning technology. The effect of pH and the amount of the $BaTiO_3$ was examined. The kinetics of PZEC degradation of methyl orange was expressed using the Langmuir−Hinshelwood model.

EXPERIMENTAL METHODS

Materials. The hydrothermal method[28] was used to synthesize $BaTiO_3$ dendrite samples of the PZEC catalyst. All

Received: November 28, 2011
Revised: May 1, 2012
Published: May 16, 2012

chemicals used as starting materials have a purity of 99.99%. Addition of 25 mL of $Ti(OC_2H_5)_4$ dropwise into 1.0 M acetic acid was applied to prepare the pre-reaction precursor $Ti(OH)_4$. The solution was settled allowing the precipitate to form in 72 h and was followed by rinsing the product with DI water and drying at 60 °C. The as-synthesized $Ti(OH)_4$ precursor and commercially available $Ba(OH)_2{\cdot}8H_2O$ were then added (Ti:Ba = 1:1 in molar ratio) into 0.25 M NaOH. After that, the mixture was placed in a Teflon cup at 60% capacity and then stirred and sealed tightly in a stainless steel autoclave (digestion bomb). The closed bomb (Parr-type) was maintained at 200 °C for 6 h under hydrothermal reaction. The bomb was then quenched in air at room temperature. The resulting white precipitate was washed with DI water to remove any adsorbed impurities and then cooled in air at room temperature. C.I. Acid Orange (AO7) was purchased from Sigma Aldrich. Figure 1 shows the structure of AO7.

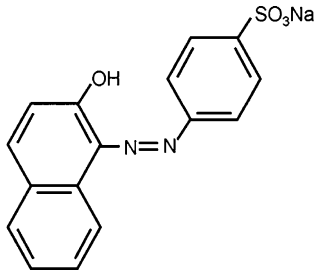

Figure 1. Chemical structure of (4-(2-hydroxy-1-naphthylazo) benzenesulfonic acid sodium salt (C.I. Acid Orange 7, Color Index Number: 15510).

$BaTiO_3$ Dendrite Characterizations. Dried samples were characterized by using powder X-ray diffraction using a Scintag Pad V Diffractometer system with Cu Kα radiation (λ = 0.1541 nm). Morphological observation and electron diffraction (ED) of particles were measured on a Philips CM 200UT Transmission Electron Microscope (TEM) with a spherical aberration coefficient (Cs) of 0.5 mm and a point-to-point resolution of 0.19 nm at an accelerating voltage of 200 kV. Scanning electron microscopy (SEM) was also conducted using a Hitachi S-3400N variable pressure scanning electron microscope with a tungsten filament that delivers at least 50 nA of beam current.

Procedures. For the PZEC degradation of 4-(2-hydroxy-1-naphthylazo)benzenesulfonic acid sodium salt (AO7, Figure 1) (Sigma Aldrich), a known concentration of a mixture of the AO7 (ranging from 10^{-6} to 10^{-4} mol/L) and $BaTiO_3$ microdendrite powder was prepared in solution. These mixtures were then transferred (5 mL) to a Pyrex glass tube, which was placed in the center of a vibration tank. Ultrasonic vibrations were carried out with a Branson 5510-MT Ultrasonic Cleaner. The pH values were controlled at the desired level using NaOH and H_2SO_4, and pH values were measured with a pH meter (Accumet XL20). The concentration of the AO7 was determined by using a spectrophotometer (UV−vis Spectrophotometer, Thermo Evolution 600) at λ_{max} = 485 nm and a calibration curve. It is important to note that all of the reactions were performed in dark conditions where we eliminated the possibility of a photocatalytic reaction. All the experiments were carried out at a temperature of 25 °C. We set the temperature at 25 °C (slightly higher than room temperature ~20 °C). The water bath temperature was monitored and controlled by adding a small amount of zero-degree water to avoid temperature generated by sonication.

RESULTS AND DISCUSSION

SEM images of hydrothermally synthesized $BaTiO_3$ dendrites are shown in Figure 2a. Precipitates of crystalline $BaTiO_3$ with perovskite structures were heated at 200 °C for 68 h in an autoclave. The crystalline $BaTiO_3$ exhibits a dendritic morphology. The primary branches of the $BaTiO_3$ dendrite are typically ~10 μm long rods that grow along [001], while secondary branches develop along a different direction than the primary rod. The secondary branches are a few micrometers in length and have a similar width and height as the primary branches. Figure 2b shows a transmission electron microscope (TEM) image of the synthesized $BaTiO_3$ dendrite. The inserted electron diffraction pattern indicates the branches in the dendrites and their crystallographic orientations. Each dendrite is a single crystal of $BaTiO_3$. The high-resolution TEM (HRTEM) image (Figure 2c) shows the (001) and (110) lattice fringes.

Piezoelectrochemical Effect. The origin of the PZEC effect, from application of an external mechanical force, was demonstrated in a previous study.[27] The strain-induced potential is generated when an external mechanical energy is applied, resulting in a bending or deformation of the $BaTiO_3$ dendrite. The strain-induced electric potential is available for the reduction and oxidation reaction via charge transfer to AO7 molecules adsorbed on the surface (Figure 3).

Spectral Changes of AO7 during PZEC Degradation. Figure 4 shows the typical change in the absorption spectra of AO7 solutions during the PZEC degradation process at different vibration times. The decrease in intensity of a peak at 485 nm (from AO7) indicates a rapid degradation of AO7 dye. The peak intensity weakened as the vibration time increased (Figure 4). Also, after 10 min, the weak band intensity at 300−310 nm started to decrease and disappeared after 30 min.

Effect of Piezoelectrochemical Phenomenon and $BaTiO_3$ Microdendrites. Figure 5 shows variation in the dye concentration as a function of time during the PZEC degradation of AO7. The removal of AO7 was negligible in the two controls (presence of $BaTiO_3$ microdendrites without ultrasonic vibration and with ultrasonic vibration but in the absence of $BaTiO_3$ microdendrites) (green and red lines in Figure 5). In contrast, when both $BaTiO_3$ microdendrites and ultrasonic vibration are present, the AO7 dye was degraded nearly 80% after 90 min of vibration. Results from our previous study of the PZEC effect show that piezoelectric materials like $BaTiO_3$ with applied external mechanical stresses are capable of the initiation of effective redox reactions including the decomposition of water[27] and the destruction of AO7. On the basis of the PZEC phenomenon, we showed that the PZEC induced degradation of organic compound in solution is initiated by deformation of the piezoelectric material in dendritic morphologies, followed by the accumulation of electrons on the material surface. Accordingly, as in the redox reactions triggered by deformation of the $BaTiO_3$ microdentrites in the aqueous solution, both water decomposition (eqs 1−9) and the PZEC degradation of AO7 (eqs 10−12) occurred simultaneously in the system.

Here we apply the ideas of photocatalytic decomposition and hypothesize that the mechanism of PZEC degradation of AO7 is analogous to that of the photocatalytic process[1,29−31] except

dx.doi.org/10.1021/jp211455z | J. Phys. Chem. C 2012, 116, 13045−13051

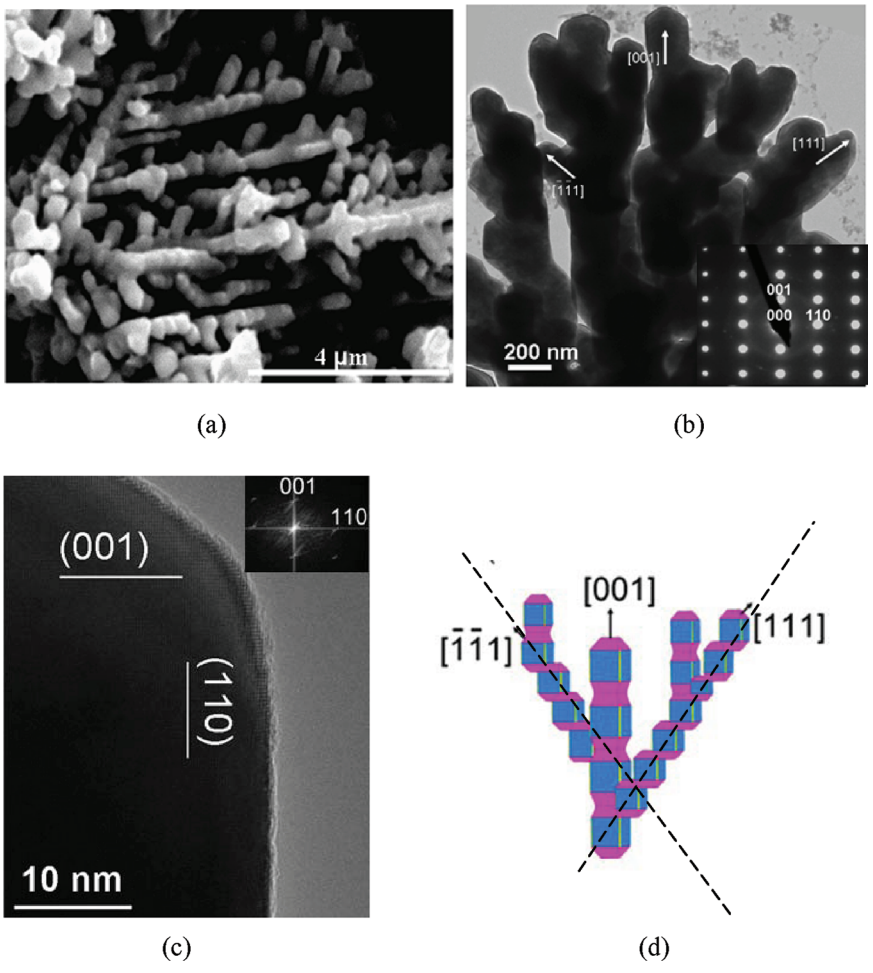

Figure 2. (a) SEM and (b) a typical TEM image of $BaTiO_3$ dendrites grown on glass substrate; (c) HRTEM image of one $BaTiO_3$ crystal in the dendrite showing (001) and (110) lattice fringes. (d) Schematic diagrams showing the shape of the $BaTiO_3$ dendrite.

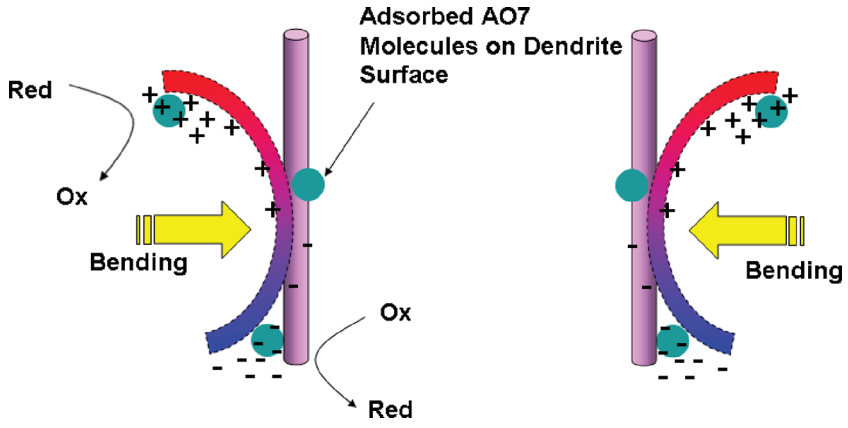

Figure 3. Schematic diagrams showing the charge development on the elongated $BaTiO_3$ microcrystals due to its piezoelectric property. AO7 are decomposed by deforming a $BaTiO_3$ microdendrite in water via oxidation−reduction reactions.

that the origins of the electron−hole pairs are now coming from the strained $BaTiO_3$ microdendrites instead of from excited photoelectrons in the conduction band.

On the anode (negatively charged sides of the $BaTiO_3$ microdendrite), the PZEC-induced electrons on the surface attract the hydrogen from the water molecules and produce hydrogen radicals $H^{\bullet}$ (eq 2) which combine with other hydrogen radicals, forming hydrogen gas (eq 3) as well as reacting with water molecules generating hydrogen gas and $OH^{\bullet}$. In contrast to the anode, the $OH^{\bullet}$ on the cathode side can be released by the holes that were accumulated on the positively charged side of the $BaTiO_3$ that attracts the electrons on the negatively charged hydroxyl group (eq 5). The $OH^{\bullet}$ radicals formed in the system are the primary cause of the degradation of AO7 in the reactions. This causes the degradation of the dye.[32,33] Additionally, the PZEC-induced holes could possibly oxidize organic molecules, forming R^{+}, or oxidize OH^{-} or H_2O to $OH^{\bullet}$ radicals.

dx.doi.org/10.1021/jp211455z | J. Phys. Chem. C 2012, 116, 13045−13051

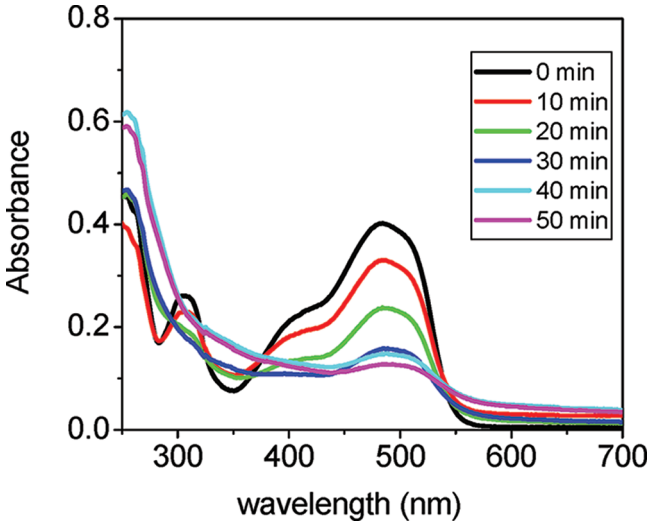

Figure 4. Spectral changes of AO7 solution during vibration in the presence of $BaTiO_3$ microdendrites; [AO7] = 5.7×10^{-5} M; $BaTiO_3$ = 0.05 g; pH neutral.

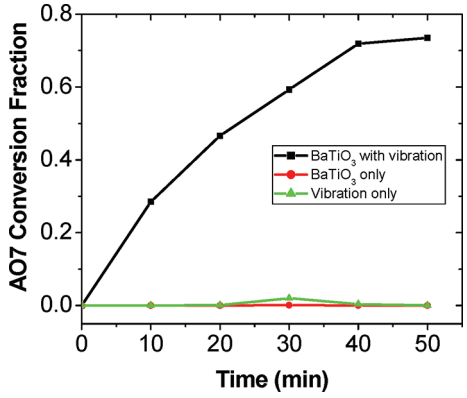

Figure 5. Effect of mechanical vibration and $BaTiO_3$ microdendrites on PZEC degradation of AO7; [AO7] = 5.7×10^{-5} M; $BaTiO_3$ = 0.10 g; pH 6.55.

$$BaTiO_3 + \text{vibration} \rightarrow BaTiO_3\ (e^- + h^+) \quad (1)$$

Anode:

$$4e^- + 4H_2O \rightarrow 4OH^- + 4H^\bullet \quad (2)$$

$$4H^\bullet \rightarrow 2H_2 \quad (3)$$

Overall:

$$4e^- + 4H_2O \rightarrow 4OH^- + 2H_2 \quad (4)$$

Cathode:

$$4OH^- \rightarrow 4e^- + 4OH^\bullet \quad (5)$$

$$2(OH^\bullet + OH^\bullet) \rightarrow 2H_2O + 2O^\bullet \quad (6)$$

$$2O^\bullet \rightarrow O_2 \quad (7)$$

Overall:

$$4OH^- \rightarrow 4e^- + 2H_2O + O_2 \quad (8)$$

Net reaction of water decomposition:

$$2H_2O \rightarrow 2H_2 + O_2 \quad (9)$$

Dye decomposition:

$$OH^\bullet + \text{dye} \rightarrow \text{degradation product of dye} \quad (10)$$

$$e^- + \text{dye} \rightarrow \text{degradation product of dye} \quad (11)$$

$$h^+ + \text{dye} \rightarrow \text{degradation product of dye} \quad (12)$$

It has been reported that the oxidative attack of AO7 leads to benzene sulfonate and naphthoquinone formation as primary products.[17] In addition, benzene sulfonic acid, sulphanilic acid, 1,4-naphthquinne, phthalic acid,[34] quinone, and 4-hydroxybenzene sulfonic acid were all identified as products of the photodegradation of AO7.[35] Overall, 22 transformation products such as 2-naphthol, 2-hydroxy-1,4-naphthoquinone, and smaller aromatic intermediates were recognized via partial and/or complete degradation of AO7.[8,30,36] While considering the degradation of AO7 via the PZEC effect, we have carefully evaluated the potential influence of sonochemical degradation, which is highly dependent on frequency and temperature.[37−39] Velegraki et al. have identified the sonochemical degradation of AO7 and its end-product using a vibration frequency of 80 kHz.[40] Accordingly, the hydroxyl radicals are formed through water sonolysis, and the radical reactions predominate with volatile and hydrophobic species in the gaseous and interface reacting with hydrophilic species in liquid bulk. In our study, however, a lower vibration frequency, 40 kHz, was applied to the system, and we found no degradation within 50 min of vibration under standard conditions. Given that AO7 is a nonvolatile compound, higher frequencies (i.e., 80 kHz) and/or higher temperatures are usually needed for degradation to occur. Since we did not observe any degradation for AO7 in both controls (without vibration or with $BaTiO_3$ only) (Figure 5), we predict that the formation of the hydroxyl radicals occurs primarily by the PZEC-induced process, leading to a different end-product of the AO7 degradation than as reported via sonolytic oxidation.

Effect of the $BaTiO_3$ Loading and Initial Dye Concentration. Figure 6 shows the effect of the amount of

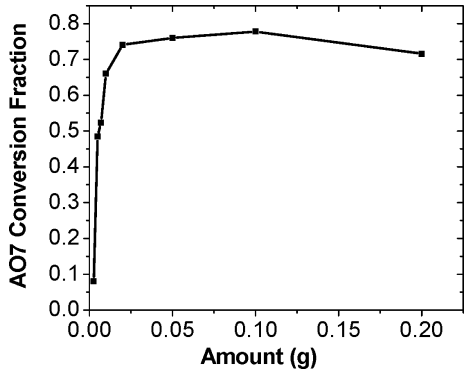

Figure 6. Effect of $BaTiO_3$ amount on PZEC degradation efficiency of Orange II at a vibration time of 60 min; [AO7] = 5.7×10^{-5} M; pH 6.55.

$BaTiO_3$ microdendrites on the PZEC degradation efficiency. The PZEC degradation efficiency increases with increasing $BaTiO_3$ concentration up to 0.025 g and then reaches a plateau followed by a slight decrease. This can be explained by the availability of strain-induced charges on the $BaTiO_3$ microdendrite surface and canceling of the opposite charges. The total active surface area increased when the amount of the

dx.doi.org/10.1021/jp211455z | J. Phys. Chem. C 2012, 116, 13045−13051

dendrites in the system was increased. As a result, the efficiency of the PZEC degradation was enhanced, while, at the same time, there was a decrease in the overall charge potential as a result of a decrease in the PZEC degradation performance. This is likely due to the increased possibility of having opposite charges in contact with each other due to collisions between dendrites.

The effect of the initial AO7 concentration on the PZEC degradation efficiency is shown in Figure 7. The efficiency of

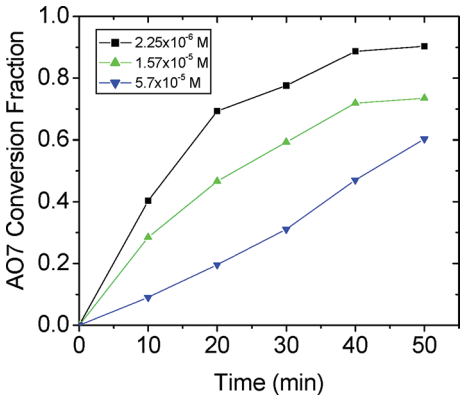

Figure 7. Effect of initial dye concentration on the PZEC degradation efficiency of AO7; $BaTiO_3$ = 0.05 g; pH 7.42.

color removal decreases as the initial dye concentration is increased. We hypothesize that more dye molecules were adsorbed on the surface of the $BaTiO_3$ dendrites when the initial concentration of the dye was increased. With a large amount of adsorbed dye present in the system, ions from the dye likely cover the active site, leading to the reduced formation of hydroxyl radicals on the dendrite surface. The difference in degradation efficiencies may be smaller if the reactions run longer. Alternatively, unlike in the photocatalytic system, the PZEC effect is an intrinsic property of the $BaTiO_3$ microdendrite, in which the screening effect of the dye ions in the PZEC degradation process does not play a major role.

Effect of pH. The effect of pH on the PZEC degradation efficiency of AO7 was tested at pH 2−11 and shown in Figure 8. The PZEC degradation efficiency was slightly decreased under alkaline conditions. The efficiency was slightly increased when the conditions were shifted toward acidic conditions, but that was followed by a decline at the lower end of pH values

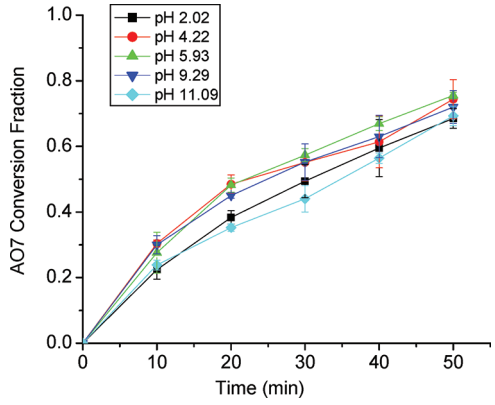

Figure 8. Effect of pH on PZEC degradation of AO7 at a vibration time of 50 min; [AO7] = 5.7 × 10^{-5} M; $BaTiO_3$ = 0.05 g.

around pH 2. The highest degradation efficiency was found in the pH range 4−8. Overall, the result, however, shows a weak pH effect on the PZEC-induced dye degradation. Here we notice that $BaTiO_3$ is stable in a wide range of pH conditions unlike ZnO, for which corrosion or dissolution will take place under low pH conditions. In addition, the mechanical energy, which is the driving force of the PZEC effect, is independent of pH values; thus, the PZEC degradation via $BaTiO_3$ dendrites performed similarly in a wide range of pH. Nevertheless, the $BaTiO_3$ surface becomes negatively charged under alkaline conditions, lowering the negatively charged dye and hydroxide anions from adsorbing onto the dendrite surface.[40] This potentially explains the slightly decreased degradation rate measured under higher pH values. By the same analogy, the increase of the degradation rate at pH 4−8 could be due to a stronger adsorption of the dye on the $BaTiO_3$ surface.

Kinetics of PZEC Degradation of AO7. The Langmuir−Hinshelwood model is used to express the PZEC degradation kinetics of AO7. Here, the PZEC induced oxidation and reduction reactions are assumed to be a rapid equilibrium process and the rate determining step involves the oxidants and reductants in a monolayer at the solid−liquid interface.[41] The PZEC degradation of AO7 using $BaTiO_3$ microdendrites exhibits a pseudo-first-order kinetics reaction with respect to the concentration of AO7:

$$-\frac{d[AO7]}{dt} = k_{obs}[AO7] \quad (13)$$

for $[AO7] = [AO7]_0$ at $t = 0$

$$\ln\left(\frac{[AO7]_0}{[AO7]}\right) = k_{obs}t \quad (14)$$

where k_{obs} is the pseudo-first-order rate constant.

Figure 9 shows a plot of $\ln[AO7]_0/[AO7]$ against time for trials using different initial concentrations of AO7. The k_{obs}

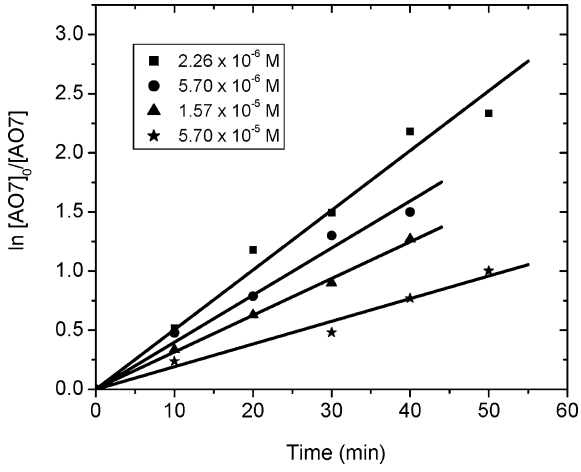

Figure 9. Determination of the pseudo-first-order kinetic rate constant, k_{obs}.

value was obtained by applying a least-squares regression. Table 1 shows the values of k_{obs} for all experiments in this study. The reaction rate proceeds by pseudo-first-order kinetics. The kinetics constant decreased as the concentration of the initial reactant increased. This is explained by the decrease in the number of available electrons on the $BaTiO_3$ surface due to the taking up of electrons by AO7, and is directly proportional with

dx.doi.org/10.1021/jp211455z | J. Phys. Chem. C 2012, 116, 13045−13051

Table 1. Kinetic Rate Constants and AO7 Conversion at the 20th Minute with Different Initial Concentrations[a]

trails	$[BaTiO_3]_0$ (g)	$[AO7]_0$ (mgl^{-1})	X_{20} (%)	$k_{obs}(min^{-1})$	$1/k_{obs}$(min)	r^2
1	0.05	20.0	19.6	0.0192	52.1	0.98
2	0.05	5.5	46.6	0.0312	32.1	0.99
3	0.05	2.0	54.5	0.040	24.4	0.98
4	0.05	0.8	69.4	0.0505	19.8	0.98

[a] X_{20}: A07 conversion fraction at the 20th minute.

the initial concentration of the AO7. The Langmuir−Hinshelwood model was used to express the relationship between the initial degradation rate (r) and the initial concentration of organic substrate for heterogeneous PZEC degradation

$$r = k_c \frac{K_{AO7}[AO7]}{1 + K_{AO7}[AO7]_0} = k_{obs}[AO7] \quad (15)$$

$$\frac{1}{k_{obs}} = \frac{1}{k_c K_{MeO}} + \frac{[AO7]_0}{k_c} \quad (16)$$

where K_{AO7} is the Langmuir−Hinshelwood adsorption equilibrium constant.

Table 1 shows the obtained values, and $1/k_{obs}$ versus $[AO7]_0$ is plotted in Figure 10. By using a least-squares best fit method,

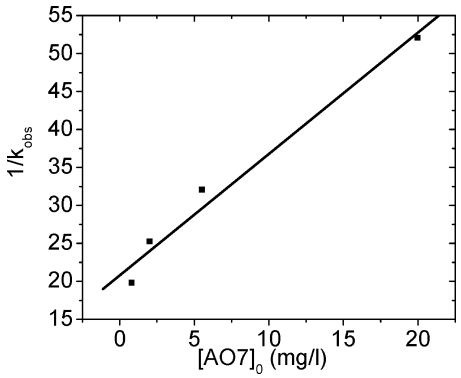

Figure 10. Determination of the adsorption equilibrium constant, K_{AO7}, and the second-order rate constant, k_c, for the Langmuir−Hinshelwood kinetic model.

the adsorption equilibrium constant (K_{AO7}) and the kinetic rate constant (k_c)[18,19] were found to be 0.149 $(mgl^{-1})^{-1}$ and 0.50 mgl^{-1} min^{-1}, respectively.

CONCLUSIONS

The piezoelectrochemical oxidation of AO7 has been studied using $BaTiO_3$ microdendrites as a PZEC catalyst. PZEC degradation was inactive when $BaTiO_3$ microdendrites and/or external mechanical energy (i.e., ultrasonic vibration) were absent in the system. The AO7 degradation results confirm that the degree of degradation of AO7 was affected by the PZEC effect and depends upon the vibration time and amount of the PZEC catalyst. PZEC degradation was affected by the initial dye concentration due to the covering of the activation sites by the dye ions. The PZEC effect, however, is based on the intrinsic properties of the materials used, in which the screening effect of the dye ions does not play an important role. Further, $BaTiO_3$ can persist at a wide range of pH values without being decomposed, although slight influences of pH were observed on the PZEC degradation performance.

AUTHOR INFORMATION

Corresponding Author

*Phone: 608-265-5887. E-mail: hfxu@geology.wisc.edu.

Notes

The authors declare no competing financial interest.

ACKNOWLEDGMENTS

This work is supported by NASA Astrobiology Institute (N07-5489), National Science Foundation (EAR-0810150), and the Graduate School and alumni of Department of Geoscience, University of Wisconsin—Madison. The authors thank Dr. Terry Morrison and two anonymous reviewers for helpful suggestions. K.-S. Hong also thanks Dr. James Robertson for providing part of summer research support.

REFERENCES

(1) Bianco-Prevot, A.; Baiocchi, C.; Brussina, M. C.; Pramauro, E.; Savarino, P.; Augugliaro, V.; Marci, G.; Palmisano, L. *Environ. Sci. Technol.* **2001**, *35*, 971−976.
(2) Houas, A.; Lachheb, H.; Ksibi, M.; Elaloui, E.; Gullard, C.; Hermann, J. M. *Appl. Catal., B* **2001**, *31*, 145−157.
(3) Saquib, M.; Muneer, M. *Dyes Pigm.* **2003**, *56*, 37−49.
(4) Zollinger, H. *Water Res.* **1991**, *27*, 63−67.
(5) Pagga, U.; Bruan, D. *Chemosphere* **1986**, *15*, 479−491.
(6) Tang, W. Z.; An, H. *Chemosphere* **1995**, *31*, 4157−4170.
(7) Kuo, W. S.; Ho, P. H. *Chemosphere* **2001**, *45*, 77−83.
(8) Galindo, C.; Jacques, P.; Kalt, A. *Chemosphere* **2001**, *45*, 997−1005.
(9) Arslan, I.; AkmehmetBalcioglou, I. *Dyes Pigm.* **1999**, *43*, 95−108.
(10) Patil, S. S.; Shinde, V. M.. *Environ. Sci. Technol.* **1988**, *22*, 1160−1165.
(11) Moore, A. T.; Vira, A.; Fogel, S. *Environ. Sci. Technol.* **1989**, *23*, 403−406.
(12) Slokar, Y. M.; Le Marechal, A. M. *Dyes Pigm.* **1998**, *37*, 335−336.
(13) Sheng, H. L.; Chi, M. L. *Water Res.* **1993**, *27*, 1743−1748.
(14) Kuo, W. G. *Water Res.* **1992**, *26*, 881−886.
(15) Balanosky, E.; Fernadez, J.; Kiwi, J.; Lopez, A. *Water Sci. Technol.* **1999**, *40*, 417−424.
(16) Feng, W.; Nansheng, D.; Yuegang, Z. *Chemosphere* **1999**, *39*, 2079−2085.
(17) Konstantinou, I. K.; Albanis, T. A. *Appl. Catal., B* **2004**, *49*, 1−14.
(18) Khodja, A. A.; Sehili, T.; Pilichowski, J.; Boule, P. *J. Photochem. Photobiol., A* **2001**, *141*, 231−239.
(19) Lizaman, C.; Freer, J.; Baeza, J.; Mansilla, H. *Catal. Today* **2002**, *76*, 235−246.
(20) Yeber, M. C.; Rodriguez, J.; Freer, J.; Baeza, J.; Duran, N.; Mansilla, H. *Chemosphere* **1999**, *39*, 1679−1688.
(21) Behnajady, M. A.; Modirshahla, N.; Hamzavi, R. *J. Hazard. Mater.* **2006**, *133*, 226−232.
(22) Liu, G.; Wu, T.; Zhao, J.; Hidaka, H.; Serpone, N. *Environ. Sci. Technol.* **1999**, *33*, 2081−2087.
(23) Zhao, J.; Wu, T.; Wu, K.; Oikawa, K.; Hidaka, H.; Serpone, N. *Environ. Sci. Technol.* **1998**, *32*.
(24) Konstantinou, I. K.; Albanis, T. A. *Appl. Catal., B* **2003**, *42*, 319−335.
(25) Reeves, P.; Ohlhausen, R.; Sloan, D.; Pamplin, K.; Scoggins, T. *Sol. Energy* **1992**, *48*, 413−420.
(26) Daneshvar, N.; Salari, D.; Khataee, A. R. *J. Photochem. Photobiol., A* **2004**, *162*, 317−322.
(27) Hong, K. S.; Xu, H.; Konishi, H.; Li, X. *J. Phys. Chem. Lett.* **2010**, *1*, 997−1002.

(28) Wang, Y.; Xu, G.; Yang, L.; Ren, Z.; Wei, X.; Weng, W.; Du, P.; Sheng, G.; Han, G. *Mater. Lett.* **2009**, *63*.
(29) Zhan, H.; Tian, H. *Dyes Pigm.* **1998**, *37*, 231−239.
(30) Bandara, J.; Mielczarski, J. A.; Kiwi, J. *Langmuir* **1999**, *15*, 7680−7687.
(31) Galindo, C.; Jacques, P.; Kalt, A. *J. Photochem. Photobiol., A* **2000**, *130*, 35−47.
(32) Daneshvar, N.; Salari, D.; Khataee, A. R. *J. Photochem. Photobiol., A* **2004**, *162*, 317−322.
(33) Konstantinou, I. K.; Albanis, T. A. *Appl. Catal., B* **2004**, *49*, 1−14.
(34) Vinodgopal, K.; Wynkoop, D.; Kamat, P. *Environ. Sci. Technol.* **1996**, *30*, 1660−1666.
(35) Bauer, C.; Jacques, P.; Kalt, A. *J. Photochem. Photobiol., A* **2001**, *140*, 87−92.
(36) Stylidi, M.; Kondarides, D. I.; Verykios, X. E. *Appl. Catal., B* **2003**, *40*, 271−286.
(37) Ince, N. H.; Tezcanli, G.; Belen, R. K.; Apikyan, I. G. *Appl. Catal., B* **2001**, *29*, 167−176.
(38) Adewuyi, Y. G. *Ind. Eng. Chem. Res.* **2001**, *40*, 4681−4715.
(39) Yezcanli-Guyer, G.; Ince, N. H. *Ultrasonics* **2004**, *42*, 603−609.
(40) Velegraki, T.; Poulios, I.; Charalabaki, M.; Kalogerakis, N.; Samaras, P.; Mantzavinos, D. *Appl. Catal., B* **2006**, *62*, 159−168.
(41) Chakrabarti, S.; Dutta, B. K. *J. Hazard. Mater.* **2004**, *112*, 269−278.